J. Fluid Mech. (2014), *vol.* 738, R3, doi:10.1017/jfm.2013.607

JFM RAPIDS
journals.cambridge.org/rapids

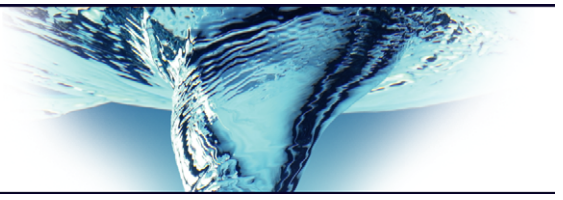

Kelvin wake pattern at large Froude numbers

Alexandre Darmon[1,2], **Michael Benzaquen**[1] **and Elie Raphaël**[1,†]

[1]PCT, UMR CNRS 7083 Gulliver, ESPCI ParisTech, 10 rue Vauquelin, 75005 Paris, France
[2]EC2M, UMR CNRS 7083 Gulliver, ESPCI ParisTech, 10 rue Vauquelin, 75005 Paris, France

(Received 11 October 2013; revised 6 November 2013; accepted 12 November 2013)

Gravity waves generated by an object moving at constant speed at the water surface form a specific pattern commonly known as the Kelvin wake. It was proved by Lord Kelvin that such a wake is delimited by a constant angle $\simeq 19.47°$. However a recent study by Rabaud and Moisy based on the observation of airborne images showed that the wake angle seems to decrease as the Froude number Fr increases, scaling as Fr^{-1} for large Froude numbers. To explain such observations they make the strong hypothesis that an object of size b cannot generate wavelengths larger than b. Without the need of such an assumption and modelling the moving object by an axisymmetric pressure field, we analytically show that the angle corresponding to the maximum amplitude of the waves scales as Fr^{-1} for large Froude numbers, whereas the angle delimiting the wake region outside which the surface is essentially flat remains constant and equal to the Kelvin angle for all Fr.

Key words: surface gravity waves, wakes/jets, waves/free-surface flows

1. Introduction

Simply by looking at a duck swimming in a pond or a cargo ship moving on a calm sea, one can clearly tell that there is something common about their wakes: they both display a familiar V-shaped pattern which only differ from each other by their dimensions. In 1887, Lord Kelvin (Kelvin 1887) proved that the wake created by an object moving at a uniform pace is always delimited by an angle equal to $\arcsin 1/3 = 19.47°$. This theory, based on stationary phase arguments, is widely used both at theoretical and technical levels (Lighthill 1978; Lamb 1993; Parnell & Kofoed-Hansen 2001; Darrigol 2005). Since Lord Kelvin, other studies have shown that two sets of waves can be distinguished in the wake: the so-called transverse waves and diverging waves (Crawford 1984; Nakos & Sclavounos 1990). Their amplitudes directly depend on the hull Froude number $Fr = V/\sqrt{gb}$, where V is the speed of the moving object, b its typical size and g is the acceleration due to gravity. It has

† Email address for correspondence: elie.raphael@espci.fr

been observed that as the Froude number increases, so does the amplitude of the diverging waves; but that of the transverse waves decreases rapidly and seems to vanish for sufficiently high Froude numbers (Lighthill 1978). Speedboats, whose range of reachable Froude number is large, typically up to $Fr \simeq 3$, experience different regimes as the Froude number is increased, eventually entering the so-called planing regime in which their drag is significantly decreased as they displace less water (Cumbertach 1958; Casling 1978; Lai & Troesch 1995). The understanding of the wave drag is of great practical importance in the ship industry for the hull design (Suzuki *et al.* 1997; Tuck, Scullen & Lazauskas 2002; Rabaud & Moisy 2013*b*). At smaller scales, the wave drag for capillary–gravity waves has also been studied extensively (Benzaquen, Chevy & Raphaël 2011; Le Merrer *et al.* 2011; Benzaquen & Raphaël 2012) and is notably of interest for insect locomotion (Chepelianskii, Chevy & Raphaël 2008; Voise & Casas 2010).

Recent experimental observations by Rabaud and Moisy have challenged the commonly accepted theory of Lord Kelvin (Rabaud & Moisy 2013*a*). Based on airborne observations of ship wakes, they show that the wake angle seems to decrease as the Froude number is increased, scaling as Fr^{-1} for large Froude numbers. To explain their observations, they make the strong hypothesis that an object of size b cannot generate wavelengths greater than b. Even though this assumption leads to consistent results regarding the experimental findings, it has not been firmly established and is open to questioning.

We here propose an explanation of such observations without the need of the above-mentioned maximum-wavelength argument. We first perform a numerical evaluation of the surface displacement induced by a moving pressure field of typical size b above the surface of water and show that two angles can be highlighted in the wake: the outer angle delimiting the wake, shown to be constant and equal to the Kelvin angle, and an inner angle corresponding to the maximum amplitude of the waves. We then analytically prove that the latter is not constant and scales as Fr^{-1} at large Froude numbers.

2. Surface displacement

In the pure gravity waves limit, the surface displacement generated by a pressure field $p(x, y)$ moving in the $-x$ direction with constant speed V can be written in the frame of reference of the moving perturbation as (Havelock 1908, 1919; Raphaël & de Gennes 1996):

$$\zeta(x, y) = -\lim_{\varepsilon \to 0} \iint \frac{\mathrm{d}k\, \mathrm{d}\theta}{4\pi^2 \rho} \frac{\hat{p}(k, \theta)\, \exp[-\mathrm{i}k(\cos\theta\, x - \sin\theta\, y)]}{c(k)^2 - V^2 \cos^2\theta + 2\mathrm{i}\varepsilon V \cos\theta / k}, \tag{2.1}$$

where $\hat{p}(k, \theta)$ is the Fourier transform of $p(x, y)$ in cylindrical coordinates, ρ is the water density and $c(k) = (g/k)^{1/2}$ is the phase speed for pure gravity waves. Let us now non-dimensionalize the problem through:

$$Z = \frac{4\pi^2 \zeta}{b}, \quad X = \frac{x}{b}, \quad Y = \frac{y}{b}, \quad K = kb, \quad \widehat{P} = \frac{\hat{p}}{\rho g b^3}, \quad \tilde{\varepsilon} = \frac{\varepsilon}{\sqrt{g/b}}, \tag{2.2}$$

where b is the typical size of the pressure field $p(x, y)$. Equation (2.1) together with (2.2) becomes:

$$Z(X, Y) = \int_{-\pi/2}^{\pi/2} \mathrm{d}\theta\, F(\theta, X, Y), \tag{2.3}$$

where:

$$F(\theta, X, Y) = -\lim_{\tilde{\varepsilon}\to 0} \int_0^\infty K\,\mathrm{d}K\, \frac{\widehat{P}(K,\theta)\,\exp[-\mathrm{i}K\,(\cos\theta\, X - \sin\theta\, Y)]}{1 - Fr^2\,K\cos^2\theta + 2\mathrm{i}\,\tilde{\varepsilon}\,Fr\,\cos\theta}. \tag{2.4}$$

Using the Sokhotski–Plemelj formula (see e.g. Appel 2007), one can write:

$$F(\theta, X, Y) = \mathrm{i}\pi\Phi(K_0, \theta, X, Y) + G(\theta, X, Y), \tag{2.5}$$

where:

$$\Phi(K, \theta, X, Y) = \frac{K\,\widehat{P}(K,\theta)\,\exp[-\mathrm{i}K\,(\cos\theta\, X - \sin\theta\, Y)]}{Fr^2\cos^2\theta}, \tag{2.6}$$

$$K_0(\theta) = \frac{1}{Fr^2\cos^2\theta}, \tag{2.7}$$

and $\int \mathrm{d}\theta\, G(\theta, X, Y)$ is a rapidly decreasing function with the distance from the perturbation. According to (2.3), (2.5), (2.6) and (2.7), and sufficiently far from the perturbation, the surface displacement is well approximated by:

$$Z(X, Y) \simeq \mathrm{i}\pi \int_{-\pi/2}^{\pi/2} \mathrm{d}\theta\, \frac{\widehat{P}(K_0(\theta), \theta)\,\exp[-\mathrm{i}(\cos\theta\, X - \sin\theta\, Y)/(Fr^2\cos^2\theta)]}{Fr^4\cos^4\theta}. \tag{2.8}$$

For a given pressure distribution one can thus obtain the surface displacement by numerically evaluating the integral in (2.8).

3. Numerical evaluation

Consider a Gaussian pressure field of typical size b, symmetrical around the origin, with corresponding Fourier transform of the form:

$$\hat{P}(K) = \exp[-K^2/(4\pi^2)]. \tag{3.1}$$

Equation (2.8) yields the profiles displayed in figure 1. Figure 1(*a*) shows relief plots of the surface displacement computed using (2.8) for different Froude numbers as a function of $\tilde{X} = X/\Lambda$ and $\tilde{Y} = Y/\Lambda$ where $\Lambda = 2\pi Fr^2$ is the dimensionless wavelength. Figure 1(*b*) displays the normalized angular envelope of the surface displacement as a function of ϕ for different Froude numbers where ϕ is the polar angle originating at the horizontal axis. The angular envelope was calculated by interpolating the maxima of the wave amplitudes over one wavelength sufficiently far from the perturbation. Figure 1(*c*) displays polar plots of the normalized angular envelope as defined in (*b*) for different Froude numbers. In all graphs the maximum of the angular envelope obtained for $\phi = \phi_{max}$ is shown with a solid red line and the Kelvin angle $\phi_K = \arcsin(1/3)$ is represented by a dashed black line. The green coloured region delimits the area in which the amplitude of the waves is above 20 % of the maximum of the angular envelope. We chose this as an arbitrary criterion for what the eye can see. It sets the error bars to the angle determined by just looking at a boat wake on an airborne picture.

First, as one can see, the wake pattern strongly depends on the Froude number. At $Fr = 0.5$ one can clearly distinguish two different sets of waves: the so-called transverse waves that are orthogonal to the trajectory, and the so-called diverging waves that are located at the edges of the wake. As the Froude number is increased the relative amplitude of the transverse waves decreases until vanishing, making way

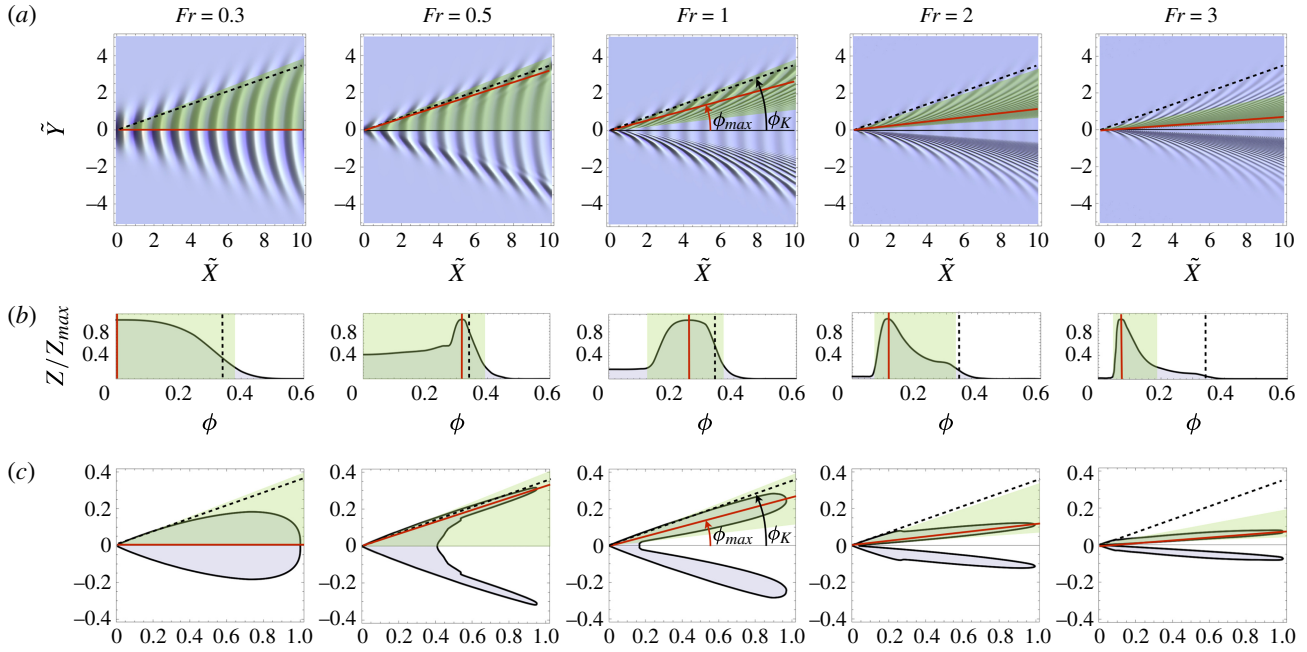

FIGURE 1. (*a*) Relief plots of the surface displacement computed using (2.8) for different Froude numbers as a function of $\tilde{X} = X/\Lambda$ and $\tilde{Y} = Y/\Lambda$ where $\Lambda = 2\pi Fr^2$ is the dimensionless wavelength. (*b*) Plot of the normalized angular envelope of the surface displacement as a function of ϕ for different Froude numbers where ϕ is the polar angle originating at the horizontal axis. The angular envelope was calculated by interpolating the maxima of the wave amplitudes over one wavelength sufficiently far from the perturbation. (*c*) Polar plot of the normalized angular envelope as defined in (*b*) for different Froude numbers. In all graphs the maximum of the angular envelope obtained for $\phi = \phi_{max}$ is shown with a solid red line and the Kelvin angle $\phi_K = \arcsin(1/3)$ is represented by a dashed black line. The green coloured region delimits the area in which the amplitude of the waves is above 20 % of the maximum of the angular envelope.

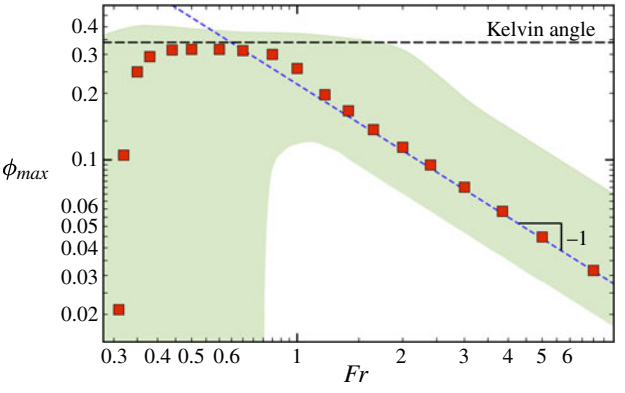

FIGURE 2. Plot of ϕ_{max} as defined in § 3 as a function of the Froude number (red squares). The green coloured region delimits the area in which the amplitude of the waves is above 20 % of the maximum of the angular envelope as defined in § 3. The dashed black line shows the Kelvin angle $\phi_K = \arcsin(1/3)$. The dashed blue line represents the asymptotic theoretical prediction at large Froude numbers as given by (4.11).

for the diverging waves. Secondly, we are interested in the evolution of ϕ_{max} as the Froude number increases. Figure 2 displays ϕ_{max} as a function of the Froude number (red squares). The green coloured region has the same meaning as that of figure 1. The dashed black line shows the Kelvin angle $\phi_K = \arcsin(1/3)$. The dashed blue line represents the asymptotic scaling Fr^{-1}. At $Fr = 0.3$ and below, the maximum of the wake angular envelope is located on the central line $\phi = 0$. A continuous transition in which the maximum is displaced to the edges of the wake $\phi_{max} \simeq \phi_K$ is observed at $Fr \simeq 0.31$. The angle ϕ_{max} then remains constant until $Fr \simeq 0.7$ before it starts to decrease, eventually scaling as Fr^{-1}. As one can see in figure 2 the green beam also scales as Fr^{-1} for large Froude numbers thus explaining the observations of Rabaud & Moisy (2013*a*). Thirdly, the waves are always confined within the Kelvin wake and always reach its outer boundary (see figure 1), even though the relatively small amplitude around this region can make it difficult to see on photographs as it might be diluted in the noise of the open sea. For a clear photograph where both the maximum amplitude angle and the Kelvin angle can be clearly identified see p. 96 of Falkovich (2011).

4. High Froude numbers

In the following we demonstrate analytically the $\phi_{max} \sim Fr^{-1}$ scaling for large Froude numbers. Surface displacement as given by (2.8) can be expressed in polar coordinates $X = R\cos\phi$, $Y = R\sin\phi$ as:

$$\breve{Z}(R,\phi) \simeq \mathrm{i}\pi \int_{-\pi}^{\pi} \mathrm{d}\theta \, \frac{\widehat{P}(K_0(\theta),\theta)\exp[-\mathrm{i}R\cos(\theta+\phi)/(Fr^2\cos^2\theta)]}{Fr^4\cos^4\theta}. \tag{4.1}$$

The integral in (4.1) is of the form $\int \mathrm{d}\theta f(\theta)\mathrm{e}^{\mathrm{i}g(\theta)}$ and may be approximated through the method of the steepest descent (Appel 2007). For $R/Fr^2 > 1$, the integrand oscillates rapidly and there are two stationary points given by $g'(\theta) = 0$:

$$\theta_1(\phi) = \tfrac{1}{2}(\arcsin(3\sin\phi) - \phi), \tag{4.2a}$$

$$\theta_2(\phi) = \tfrac{1}{2}(\pi - \arcsin(3\sin\phi) - \phi). \tag{4.2b}$$

Note that at the Kelvin angle $\phi = \phi_K = \arcsin(1/3)$, the two points θ_1 and θ_2 coalesce and thus the saddle-point method will not be accurate in the vicinity of $\phi = \phi_K$. The calculation for two coalescing saddle points (Johnson 1997) will not be developed here as our aim is to study the behaviour of ϕ_{max} at large Froude numbers for which *a priori* ϕ_{max} is far below ϕ_K. In this range both saddle points can safely be considered independently. Hence, far below ϕ_K one can write:

$$\check{Z}(R, \phi) \simeq \mathrm{i}\pi \left(\check{Z}_1(R, \phi) + \check{Z}_2(R, \phi) \right), \tag{4.3}$$

where:

$$\check{Z}_j(R, \phi) = \sqrt{\frac{2\pi}{\left|\partial_\theta^2 g(R, \theta_j, \phi)\right|}} f(\theta_j) \exp\left[\mathrm{i} \left(g(R, \theta_j, \phi) + (\pi/4) \right) \right], \tag{4.4}$$

where θ_j, $j \in \{1, 2\}$, are implicit function of ϕ as defined through (4.2) and where:

$$f(\theta) = \frac{\widehat{P}(K_0(\theta), \theta)}{Fr^4 \cos^4\theta}, \tag{4.5}$$

$$g(R, \theta, \phi) = -\frac{R\cos(\theta + \phi)}{Fr^2 \cos^2\theta}. \tag{4.6}$$

One can easily check that far below ϕ_K the function $\check{Z}_1$ exclusively defines the transverse waves whereas $\check{Z}_2$ exclusively defines the diverging waves. Let us again take the Gaussian pressure field of (3.1). As an effect of the normalization of the pressure field, both functions decrease as the Froude number is increased. Yet, the amplitude of the $\check{Z}_1$ waves scales as Fr^{-4} whereas the amplitude of the $\check{Z}_2$ waves scales as $Fr^{-3/2}$ thus decreasing more slowly. This explains why the transverse waves vanish compared to the diverging waves for large Froude numbers. Let us now thus focus on the $\check{Z}_2$ function. At a given R, the angular envelope function of $\check{Z}_2$ is given by:

$$h(R, \phi) = \sqrt{\frac{2\pi}{|\partial_\theta^2 g(R, \theta_2, \phi)|}} f(\theta_2), \tag{4.7}$$

where θ_2 and g are defined through (4.2) and (4.6). Figure 3 displays $\check{Z}_2(R = 10\Lambda, \phi)$ as given by (4.4) as a function of ϕ for different Froude numbers. Their angular envelopes given by (4.7) are shown with a solid black line. For small angles ϕ, (4.7) reduces to:

$$h(R, \phi) \simeq \sqrt{\frac{\pi}{16R}} \frac{1}{Fr^3 \phi^{5/2}} \widehat{P}\left(\frac{1}{4Fr^2\phi^2}, \frac{\pi}{2} - 2\phi \right). \tag{4.8}$$

The angle ϕ_{max} corresponding to the maximum of the amplitude is obtained by solving $\partial_\phi h = 0$. In the case of an axisymmetric pressure field, this yields:

$$5\widehat{P}(u) + 4u\,\widehat{P}'(u) = 0, \tag{4.9}$$

where $u = 1/(2Fr\,\phi)^2$. The solution u^* of (4.9) being a pure number, the angle ϕ_{max} scales as:

$$\phi_{max} \sim \frac{1}{Fr}, \tag{4.10}$$

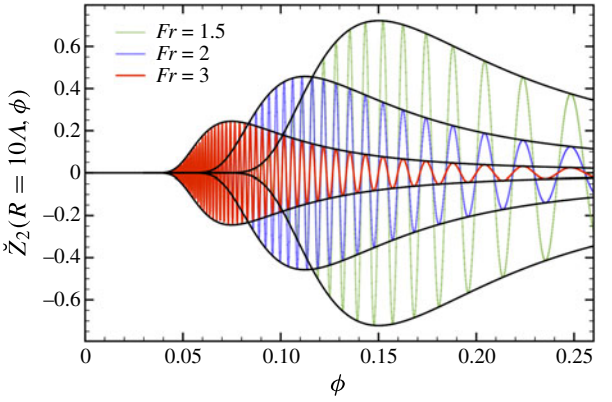

FIGURE 3. Plot of $\check{Z}_2(R = 10\Lambda, \phi)$ as given by (4.4) with the Gaussian pressure field of (3.1), where $\Lambda = 2\pi Fr^2$, as a function of ϕ for different Froude numbers. Their angular envelopes given by (4.7) are shown with a solid black line.

since $u^* = 1/(2Fr\,\phi_{max})^2$. In the particular case of the Gaussian pressure field introduced in (3.1), one has:

$$\phi_{max} = \frac{1}{40^{1/4}\sqrt{\pi}}\,\frac{1}{Fr}. \tag{4.11}$$

As one can see on figure 2, this prediction (blue line) fits perfectly the numerical results at large Froude numbers.

5. Conclusion

In this paper we performed a theoretical study of the Kelvin wake pattern generated by a moving perturbation and focused on the large Froude number regime. We showed that the angle delimiting the wake region outside which the surface is unperturbed remains constant and equal to the Kelvin angle for all Froude numbers. However, a different angle corresponding to the maximum of the amplitude of the waves can be identified. Considering an axisymmetric pressure field, we analytically showed that this angle scales as Fr^{-1} for large Froude numbers thus behaving as a Mach angle, as highlighted by Rabaud & Moisy (2013*a*) in their observations of real ships.

Acknowledgements

We wish to thank V. Bacot, O. Dauchot, S. Ellingsen, G. Falkovich, T. Salez and L. Tuckerman for very interesting discussions.

References

APPEL, W. 2007 *Mathematics for Physics and Physicists*. Princeton University Press.

BENZAQUEN, M., CHEVY, F. & RAPHAËL, E. 2011 Wave resistance for capillary gravity waves: Finite-size effects. *Europhys. Lett.* **96** (3), 34003.

BENZAQUEN, M. & RAPHAËL, E. 2012 Capillary-gravity waves on depth-dependent currents: Consequences for the wave resistance. *Europhys. Lett.* **97** (1), 14007.

CASLING, E. M. 1978 Planing of a low-aspect-ratio flat ship at infinite Froude number. *J. Engng Maths* **12**, 43–57.

CHEPELIANSKII, A. D., CHEVY, F. & RAPHAËL, E. 2008 Capillary-gravity waves generated by a slow moving object. *Phys. Rev. Lett.* **100** (7), 074504.

CRAWFORD, F. 1984 Elementary derivation of the wake pattern of a boat. *Am. J. Phys.* **52**, 782–785.

CUMBERTACH, E. 1958 Two-dimensional planing at high Froude number. *J. Fluid Mech.* **4**, 466–478.

DARRIGOL, O. 2005 *Words of Flow: A History of Hydrodynamics from the Bernoullis to Prandtl*. Oxford University Press.

FALKOVICH, G. 2011 *Fluid Mechanics — A Short Course for Physicists*. Cambridge University Press.

HAVELOCK, T. H. 1908 The propagation of groups of waves in dispersive media, with application to waves on water produced by a travelling disturbance. *Proc. R. Soc.* A **95**, 354.

HAVELOCK, T. H. 1919 Periodic irrotational waves of finite height. *Proc. R. Soc. Lond.* A **95**, 38–51.

JOHNSON, R. S. 1997 *A Modern Introduction to the Mathematical Theory of Water Waves*. Cambridge University Press.

KELVIN, LORD 1887 On ship waves. *Proc. Inst. Mech. Engrs* **38**, 409–434.

LAI, C. & TROESCH, A. W. 1995 Modelling issues related to the hydrodynamics of three-dimensional steady planing. *J. Ship Res.* **39**, 1–24.

LAMB, H. 1993 *Hydrodynamics*, 6th edn. Cambridge University Press.

LE MERRER, M., CLANET, C., QUÉRÉ, D., RAPHAËL, E. & CHEVY, F. 2011 Wave drag on floating bodies. *Proc. Natl Acad. Sci.* **108** (30), 15064–15068.

LIGHTHILL, J. 1978 *Waves in Fluids*. Cambridge University Press.

NAKOS, D. E. & SCLAVOUNOS, P. D. 1990 On steady and unsteady ship wave pattern. *J. Fluid Mech.* **215**, 263–288.

PARNELL, K. E. & KOFOED-HANSEN, H. 2001 Wakes from large high-speed ferries in confined coastal waters: Management approaches with examples from New-Zealand and Denmark. *Coastal Management* **29**, 217–237.

RABAUD, M. & MOISY, F. 2013*a* Ship wakes: Kelvin or mach angle? *Phys. Rev. Lett* **110**, 214503.

RABAUD, M. & MOISY, F. 2013*b* *Narrow ship wakes and wave drag for planning hulls. Innov-Sail, Lorient, 26–28 June*.

RAPHAËL, E. & DE GENNES, P.-G. 1996 Capillary gravity waves caused by a moving disturbance: wave resistance. *Phys. Rev.* E **53** (4), 3448–3455.

SUZUKI, K., NAKATA, Y., IKEHATA, M. & KAI, H. 1997 Numerical prediction on wave making resistance of high speed trimaran. In *Fourth International Conference on Fast Sea Transportation, Sydney, 21–23 July*.

TUCK, E. O., SCULLEN, D. C. & LAZAUSKAS, L. 2002 Wave patterns and minimum wave resistance for high-speed vessels. In *24th Symposium on Naval Hydrodynamics, Fukuoka, Japan, 8–13 July*.

VOISE, J. & CASAS, J. 2010 The management of fluid and wave resistances by whirligig beetles. *J. R. Soc. Interface* **7**, 343.